Scientific paper

Impact-Resistant Behavior of Steel-Fiber-Reinforced Porosity-Free Concrete Beam

Yusuke Kurihashi[1*], Katsuya Kono[2] and Masato Komuro[3]

Received 19 July 2019, accepted 22 March 2020 doi:10.3151/jact.18.146

Abstract

Porosity-free concrete (PFC) is a newly developed ultra-high-strength concrete with a compressive strength of 400 MPa. PFC reduces the weight of bridge superstructures, protects against collisions with flying objects, increases seismic-resistant capacity, and improves long-term durability. At present, basic material properties of PFC, such as compressive strength, tensile strength, and tensile toughness have been revealed. However, impact resistance has not been examined. In this study, in order to investigate the impact-resistant behavior of steel-fiber-reinforced PFC, falling-weight impact-loading tests were conducted on a PFC beam, considering the mixing ratio of steel fiber and the height of falling-weight as variables. To investigate the effects of compressive strength on the impact-resistant behavior of the concrete beam, tests using high-strength concrete (HC) with a compressive strength of 100 MPa were also conducted as general high-strength concrete. From this experimental study, the following results were obtained: 1) impact resistance capacity of the PFC beam can be more drastically improved by mixing 2 vol.% of steel fiber compared to the HC beam; 2) bonding resistance between PFC and steel fiber could play an important role in upgrading the impact resistance. PFC mixed with 2 vol.% steel fiber could be used as an effective reinforcement material for impact protection structures.

1. Introduction

Ultra-high-strength cementitious composites can reduce the size of the cross section of concrete structures, thus enabling weight reduction. Accordingly, it is possible to reduce the construction cost, shorten the construction period, and increase the span length, because the cross sections of the substructure and foundation can be made smaller. In addition, as the long-term durability of the material is relatively high, it can reduce the frequency of regular inspection and repair works for concrete structure. Thus, it is expected to reduce the total budget, considering the life cycle cost. Presently, many cementitious materials mixed with short fibers have also been developed for preventing brittle fractures and improving ductility. Walraven (2009) introduced practical applications, material properties, and a structural design method for high-performance fiber-reinforced concrete. The Japan Concrete Institute (JCI 2012) demonstrated many innovative applications for various fiber-reinforced cementitious composites (FRCCs). The Japan Society of Civil Engineers (JSCE 2015) proposed a structural design method for infrastructures using FRCC. Kabele *et al.* (2015) numerically investigated the flexural behavior of a notched beam made with high-strength FRCC.

For example, ultra-high-strength fiber-reinforced concrete (UFC) with a compressive strength of 200 MPa has been utilized practically in the world. The Japan Society of Civil Engineers has also specified a structural design method for UFC application (JSCE 2004). Fujikake *et al.* (2006a, 2006b, 2006c) proposed nonlinear analysis for a beam based on rapid tensile and bending test results. Ma *et al.* (2016) investigated the relationship between applied load and permeability of UFC. Sugano *et al.* (2007) indicated the applicability of UFC to earthquake resistant structures based on cyclic loading tests of a pier model. Limpaninlachat *et al.* (2017) proposed a method for the evaluation of load-carrying capacity for a beam, with UFC panels placed on both side-surfaces.

Moreover, in recent years, ultra-high-strength concrete, which achieves a compressive strength of 450 MPa or more, has been developed in Japan. This concrete, called porosity-free concrete (PFC), is formulated based on the close-packing theory, and its voids are minimized as much as possible by performing water absorption treatment and heat curing at the time of demolding (Kono *et al.* 2015, 2016a, 2016b). A previous study conducted material tests on the compressive and tensile properties of fiber-reinforced PFCs and quantitatively evaluated the compressive stress-strain curve and the softening characteristics of tensile stress after cracking (Yanagida *et al.* 2016).

On the other hand, in the aforementioned UFC, focusing on material properties with high strength and excellent toughness performance, research on applicability to impact-resistant structures is being promoted (Takahashi

[1]Associate Professor, Department of Geosciences and Civil Engineering, Kanazawa University, Japan. *Corresponding author, *E-mail*: kuri@se.kanazawa-u.ac.jp
[2]Manager, Multi-Function Concrete Team, R&D Department II, Central Research Laboratory, Taiheiyo Cement Corporation, Japan.
[3]Professor, Civil Engineering Research Unit, College of Design and Manufacturing Technology, Muroran Institute of Technology, Japan.

Table 1 List of materials used for concrete.

Type	Name	Abbreviation	Component and physical properties
Binder (B)	Low heat Portland cement	L	Specific surface area: 3330 cm^2/g, Density: 3.24 g/cm^3
	Fine quartz powder	Q	Density: 3.24 g/cm^3, Purity: 99.9% or more
	Silica fume	SF	Specific surface area: 20 m^2/g, Density: 2.29 g/cm^3
Fine aggregate	Silica sand	S	Maximum dimension: 0.3 mm, Density: 2.61 g/cm^3
Short fiber	Steel fiber	F	Diameter: 0.2 mm, Length: 15 mm, Density: 7.84 g/cm^3 Tensile strength: 2800 MPa, Tensile modulus of elasticity: 210 GPa
Admixtures	High-performance water-reducing agent	SP	Polycarboxylic-acid-based material
	De-foaming agent	DF	Polyglycol-based material

Table 2 Mix proportions.

Name	W/B (%)	Unit quantity (kg/m^3)								Flow[*2] (mm)	Air content[*3] (%)	Compressive strength[*4] (MPa)
		W	B			S	F	SP[*1]	DF[*1]			
			L	Q	SF							
PFC0	15	199	876	347	102	927	0	B × 2.5%	B × 0.02%	280	3.9	404
PFC1							78 (1 vol.%[*5])			269	3.9	375
PFC2							157 (2 vol.%[*5])			276	3.2	374
HC0	33	271	639	253	75	927	0	B × 0.4%	B × 0.02%	185	3.2	112
HC1							78 (1 vol.%[*5])	B × 0.45%		204	2.1	115
HC2							157 (2 vol.%[*5])	B × 0.5%		214	2.0	115

*1: Partial substitution on part of W; *2: Value by flow test not giving drop vibration (in accordance with JIS A 5201); *3: Air chamber pressure method; *4: Cylindrical specimen with dimensions ϕ 50 × 100 mm; *5: Outer percentage.

et al. 2013; Beppu *et al.* 2013, 2016; Ueno *et al.* 2015, 2017), and studies on practical use are being conducted (JSDFE 2018). Therefore, it is considered that mixing fibers with PFC, which has higher compressive strength, may be useful as a material for impact-resistant structures and their repair and reinforcement. However, the impact resistance of fiber-reinforced PFC has never been studied to date. If such material property can be revealed, fiber-reinforced PFC could be used as an effective reinforcing material for protective structures.

From such a background, in this study, in order to collect basic data on the impact-resistant behavior of fiber-reinforced PFC, falling-weight impact-loading tests were conducted on PFC formed into a beam shape.

2. Outline of the experiment

2.1 Outline of the specimen

2.1.1 Materials and mix proportions

Table 1 lists the materials used for PFC and high-strength concrete (HC). **Table 2** gives the mix proportions for those materials. As shown in the table, low thermal Portland cement (L), fine quartz powder (Q), and silica fume (SF) were used as the binder (B), and silica sand (S) was used as the fine aggregate. Furthermore, high-performance water-reducing agent (SP) and de-foaming agent (DF) were used for achieving both ultra-high strength and appropriate workability. In addition, steel fiber (F) was mixed at 1 or 2 vol.% (outer percentage). For the details of the concept of mix design, please refer to Kono *et al.* (2015). Compressive strength tests were also conducted in accordance with JIS A 1108 (JIS 2018), using a cylindrical specimen with diameter 50 mm and height 100 mm.

2.1.2 Mixing method and curing method

For PFC and HC, each of the materials W, B, S, SP, and DF was added to an Omni mixer (volume = 30 L, Tiger-Chiyoda Machinery) and mixed for 8 min, after which F was added and mixed for 2 min. Then, it was cast into a specified formwork, sealed, cured in the formwork while being maintained at a standard temperature of 20°C, and demolded at a material age of 48 h. Furthermore, in the case of PFC, after demolding, to promote the hydration of the cement, 1) the specimen was placed in a closed container, 2) negative pressure was applied by using a vacuum pump, and then 3) water was introduced into the container. The de-aeration time was 30 min after the water level reached the top surface of the specimen (see **Fig. 1**).

The specimens subjected to the abovementioned water absorption treatment were cured with steam (heating rate = 15°C/h, maximum temperature = 90°C, maximum temperature holding time = 48 h, and cooling rate = 15°C/h), after which they were heated and cured (heating rate = 60°C/h, maximum temperature = 180°C,

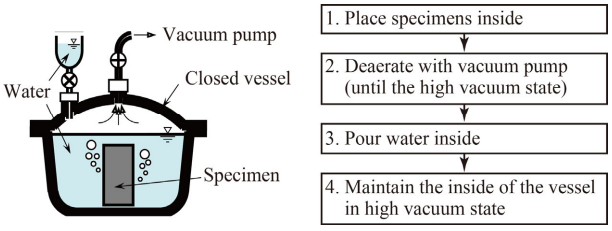

Fig. 1 Outline of degassing and water absorption treatment (Yanagida *et al.* 2016).

maximum temperature holding time = 48 h, and cooling rate = 60°C/h) (see **Fig. 2**).

2.1.3 Mechanical characteristics of PFC and HC

The compressive strengths of PFC and HC are as given in **Table 2**. In the case of PFC, it is seen that the compressive strength is reduced by approximately 10% owing to the inclusion of steel fibers. In contrast, each HC has almost the same strength, regardless of the steel fiber content ratio.

Here, the mix proportions for PFC1/PFC2 correspond to T-CPC-1 and T-CPC-2 according to Yanagida *et al.*'s study (2016). As a reference, **Fig. 3** shows the test results for the compressive stress-strain relationship, the load (P), and crack mouth opening displacement (CMOD) curve by a three-point bending test of the notch beam and tension-softening curve determined from the P-CMOD curve. These results show that the compressive strengths are almost the same, irrespective of the steel fiber content ratio V_f, but the tensile ductility increases with increasing V_f. These experimental results are described by Yanagida *et al.* (2016) in detail. Furthermore, as the matrix of PFC is tightly packed, its durability is higher than that of HC. Therefore, by applying PFC to concrete structures, maintenance-free operation can be fully expected.

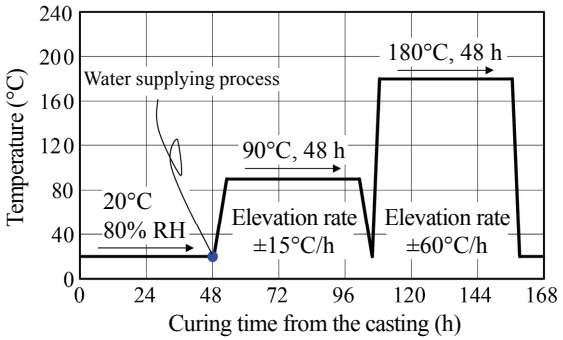

Fig. 2 Curing process (Yanagida *et al.* 2016).

2.2 Outline of static and impact-loading tests

2.2.1 List of specimens

Table 3 gives a list of specimens used in this experiment. The number of specimens is 22, taking types of concrete, mixing ratio of steel fiber, loading method, and weight drop height as variables. The first item of the test specimen name indicates the type of concrete and steel fiber content V_f (vol.%). The number attached to

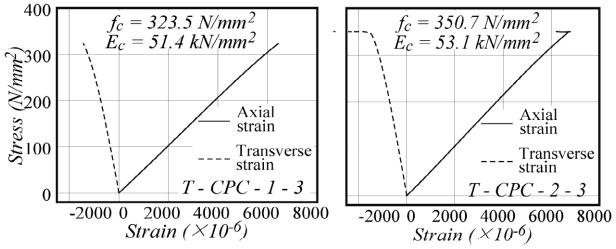

(a) Compressive stress–strain relationship

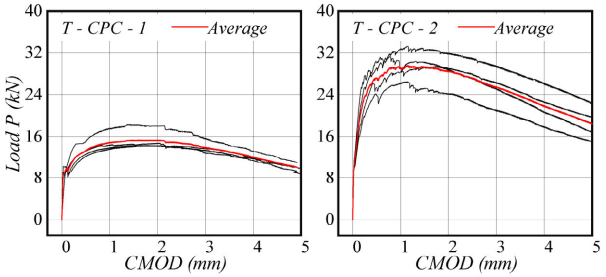

(b) Load–opening crack mouth displacement (P–CMOD) curve

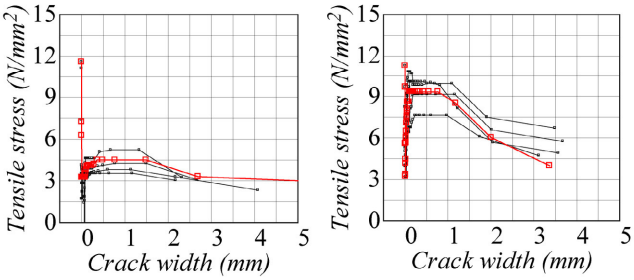

(c) Tension softening curve determined from P–CMOD curve

Fig. 3 Reference data on material properties of PFC (Yanagida *et al.* 2016).

Table 3 List of specimens.

Specimen	Concrete type	Steel fiber content (vol.%)	Weight drop height H (mm)
PFC0-H1	PFC	0	1
PFC0-H2			2
PFC0-H3			3
PFC1-S		1	(Static loading)
PFC1-H100			100
PFC1-H200			200
PFC1-H300			300
PFC2-S		2	(Static loading)
PFC2-H100			100
PFC2-H200			200
PFC2-H300			300
HC0-H1	HC	0	1
HC0-H2			2
HC0-H3			3
HC1-S		1	(Static loading)
HC1-H100			100
HC1-H200			200
HC1-H300			300
HC2-S		2	(Static loading)
HC2-H100			100
HC2-H200			200
HC2-H300			300

the letter H in the second item signifies the weight drop height H (mm). In the case of a static loading test, the second item is the letter S.

Figure 4 shows the dimensions of the specimen. The specimens used in this study have cross-sectional dimensions (width × height) of 100 × 25 mm and a net span length of 500 mm. Some target markers were placed on the side surface of the specimen for image analysis with a high-speed camera, as described later. In this experiment, the fresh PFC was cast exploiting the self-compacting ability of the PFC, flowing from one end of the mold to the other.

2.2.2 Test method and measurement items

Figure 5 shows the setup of the static loading test. The static loading test was conducted via the three-point bending test method, with the loading position at the center of the span. The load was applied by deflection control with a loading speed of 0.12 mm/min. The measurement items were the applied load and deflection of the loading point.

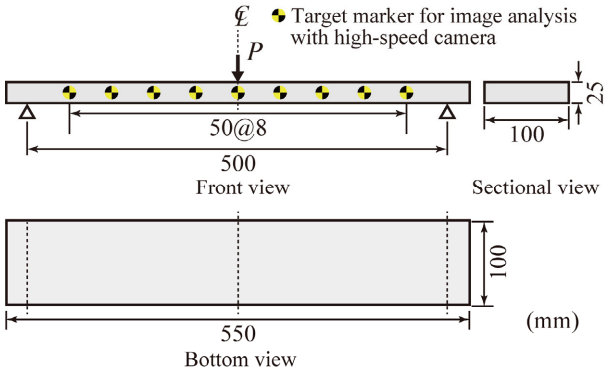

Fig. 4 Dimensions of specimen (unit: mm).

Figure 6 shows the impact-loading test setup. In this test, a single loading method was applied, in which a steel weight with a mass of 20 kg and a tip diameter of 60 mm is freely dropped at the center of the span only once from the specified drop height. In addition, both supporting points of the specimen are allowed rotation and restrained rebounding. It is similar to a pinned support. Among the measurement items, the weight impact force and reaction force were recorded by a digital memory system with a sampling time of 0.01 ms.

The deflection and relative distance of the target markers were calculated from the amount of movement of the target marker attached to the side surface of the specimen, using the image captured by a high-speed camera by the progressive scan method, the sensor resolution being 1024 × 1024 pixels. The frame rate was 2000 frames per second. In this experiment, the size of one pixel was set as approximately 0.5 mm × 0.5 mm, and the movement amount of the target marker was evaluated by using the general-purpose image analysis software ViewPoint Standard (IDT). The resolution of the movement was confirmed to be approximately 0.05 mm. After the experiment, the crack patterns of the specimen were observed and recorded.

3. Results of static loading test

3.1 Load-deflection relationship

Figure 7 compares the load-deflection relationship of fiber-reinforced PFC and HC beams. According to the

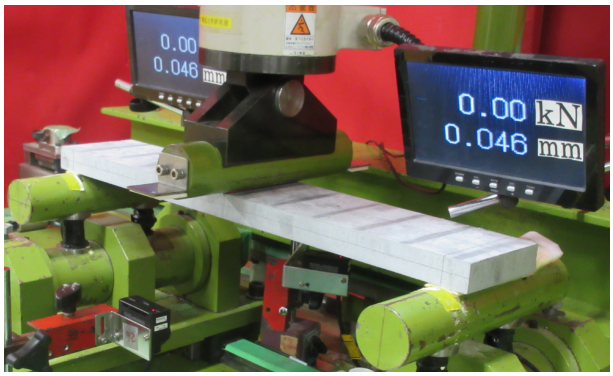

Fig. 5 Setup of static loading test.

Fig. 6 Setup of impact-loading test.

figure, in all specimens, the load linearly increases from 0.5 to 1.0 mm deflection, and then the increasing rate of the static load decreases or the load gradually decreases. This means that the bending crack opened in the vicinity of the loading point, and after that the opening of the crack could be restricted by the bridging effect of the steel fiber.

In the case of PFC1-S with a fiber content of 1 vol.%, the load slightly fluctuates around a median value of approximately 1.6 kN when the deflection is in the range of 1.5 to 10 mm. This implies that steel fibers restrain the crack opening but those are gradually pulled out from the matrix. On the other hand, in the case of PFC2-S with a fiber content of 2 vol.%, the static load increases even after the occurrence of bending cracks, and then it decreases after reaching 8 mm in deflection. This is because steel fibers come out after bending crack opening, but their bonding resistance is greater than that of PFC1-S.

On the other hand, in the case of HC beams, the bending crack load and the maximum load are smaller than those for PFC beams are. From these results, it is clear that the tensile strength and bonding resistance to the steel fiber for HC are lower than those for PFC because the compressive strength of HC is smaller than that of PFC. This means that the fine microstructure of the matrix of PFC effectively acts to improve the bonding resistance to the steel fiber.

In addition, it was revealed that the bending strength improves by mixing steel fibers, regardless of the type of concrete.

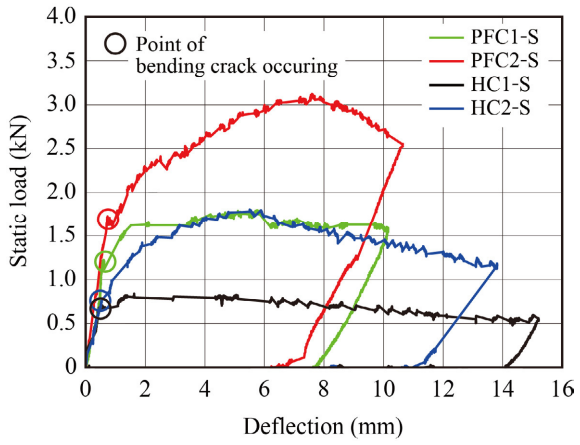

Fig. 7 Load-deflection relationship.

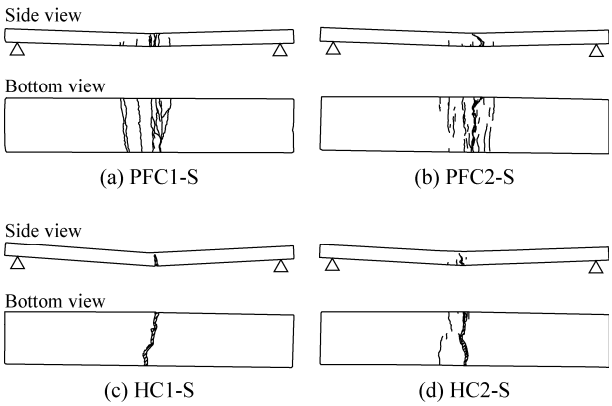

Fig. 8 Crack distribution after static loading test.

3.2 Crack distribution characteristics

Figure 8 shows the crack distribution after the static loading test. From the figure, it can be seen that, in the cases of PFC1/2-S, several fine cracks are generated, whereas in the cases of HC1/2-S, the cracks near the loading point are largely opened. Thus, it is seen that the crack dispersion effect of PFC is greater than that of HC. This means that the bonding strength of PFC1/2-S to steel fibers is higher than that of HC1/2-S, and the bridging effect is also more effectively exhibited.

4. Results of impact-loading test

4.1 Time history of response waveform

Figure 9 shows the time history of the response waveform for each specimen. In this experiment, some beams were deformed into a V-shape, and the member rotation angle significantly increased. For these cases, the experimental results of the reaction force are not shown because those results could not be evaluated properly.

As seen in **Fig. 9(a)**, the impact forces of PFC/HC0 beams are small because the drop height of those beams is low, in which it was H = 1, 2 and 3 mm. In the experiment, both specimens collapsed with H = 3 mm, and the beams were split in two parts. The impact force of steel-fiber-reinforced PFC/HC beams shows the waveform with large amplitude and very short duration, and then, the waveform with the small amplitude is generated several times. The maximum amplitude of these beams is approximately 10 times larger than that of the PFC/HC0 beams without the steel fiber.

From **Fig. 9(b)**, it can be seen that the reaction force waves of the PFC/HC0 beams exhibit a triangular shape with a maximum amplitude of about 2 kN and duration of about 10 ms. Moreover, its maximum amplitude is smaller than that in the case of fiber-reinforced PFC/HC beams. In the case of fiber-reinforced PFC/HC beams, sinusoidal half waves are excited. It indicates that the beams behave elastically. Further, comparing the case of the same drop height (H = 100 mm), it is seen that the main wave duration tends to be shorter as the compressive strength is higher and the fiber mixing ratio is higher. This implies that the natural vibration period becomes shorter as the flexural rigidity of the beam increases. Based on vibration theory, the natural vibration period T is inversely proportional to the square root of flexural rigidity EI, as given below (Takemoto *et al.* 2000).

$$T = 2\pi\sqrt{\frac{m}{\alpha EI}} \tag{1}$$

where T is the natural vibration period, m is the equivalent mass of beam, EI is the flexural rigidity and α a

constant determined by boundary conditions. In this experiment, assuming the duration of the reaction force waveform as the natural vibration period T by increasing the steel fiber content ratio from 1 vol.% to 2 vol.%, T for PFC and HC beams becomes 0.78 and 0.92 times as long, respectively. This means that the flexural rigidity EI for PFC and HC beams is improved by 1.64 and 1.18 times, respectively.

From **Fig. 9(c)**, the deflection waves of PFC/HC0 beams show the maximum amplitude of 1 mm or less for drop height H = 1 and 2 mm. In the case of H = 3 mm, the amplitudes are about 5 mm, and at this point

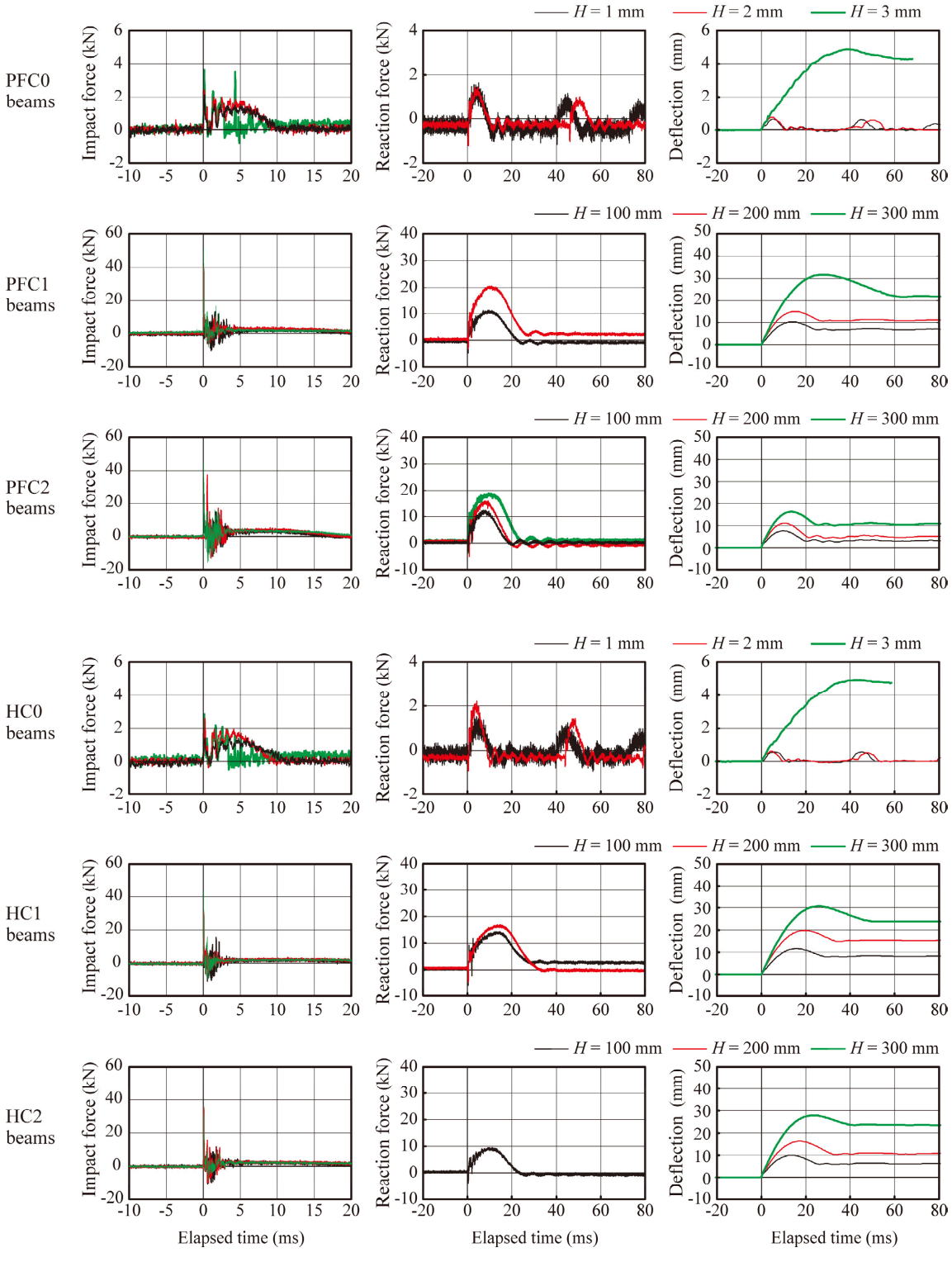

Fig. 9 Time-history response waveforms.

the beams are completely collapsed. In the case of the fiber-reinforced PFC/HC beams, after reaching the maximum amplitude, the deflection is restored. In addition, the maximum and residual deflections are the smallest for the PFC2 beam among all beams. From this result, it can be seen that the impact resistance of the PFC2 beam in this study is the highest.

4.2 Crack distribution characteristics

Figure 10 shows the crack distribution on the side and bottom surfaces of each specimen after the impact-loading test. In addition, residual deflection δ_r is also shown. From the figure, it can be seen that the number of cracks increases, and the cracks open widely near the loading point as the drop height H increases, regardless of the type of specimen.

PFC/HC0 beams collapsed at the drop height H = 3 mm. **Figure 11** shows the crack surface of both specimens. It can be seen from this photograph that the crack surface of the PFC0-H3 beam is smoother than that of the HC0-H3 beam. This means that the PFC0-H3 beam failed more than the HC0-H3 beam owing to brittleness because of the high compressive strength of PFC.

Comparison of the distribution of cracks in the fiber-reinforced PFC/HC beams shows that the cracks observed in HC beams are wider than those in PFC beams are and that the cracks near the loading point tend to open widely. As a reference, **Fig. 12** shows the crack opening condition of the specimens HC1/2-H300. On the other hand, in the case of PFC beams, many fine cracks tend to occur in the wide region. These tendencies resemble the results of static loading tests described before.

In addition, in the case of PFC2-H300, it can be seen

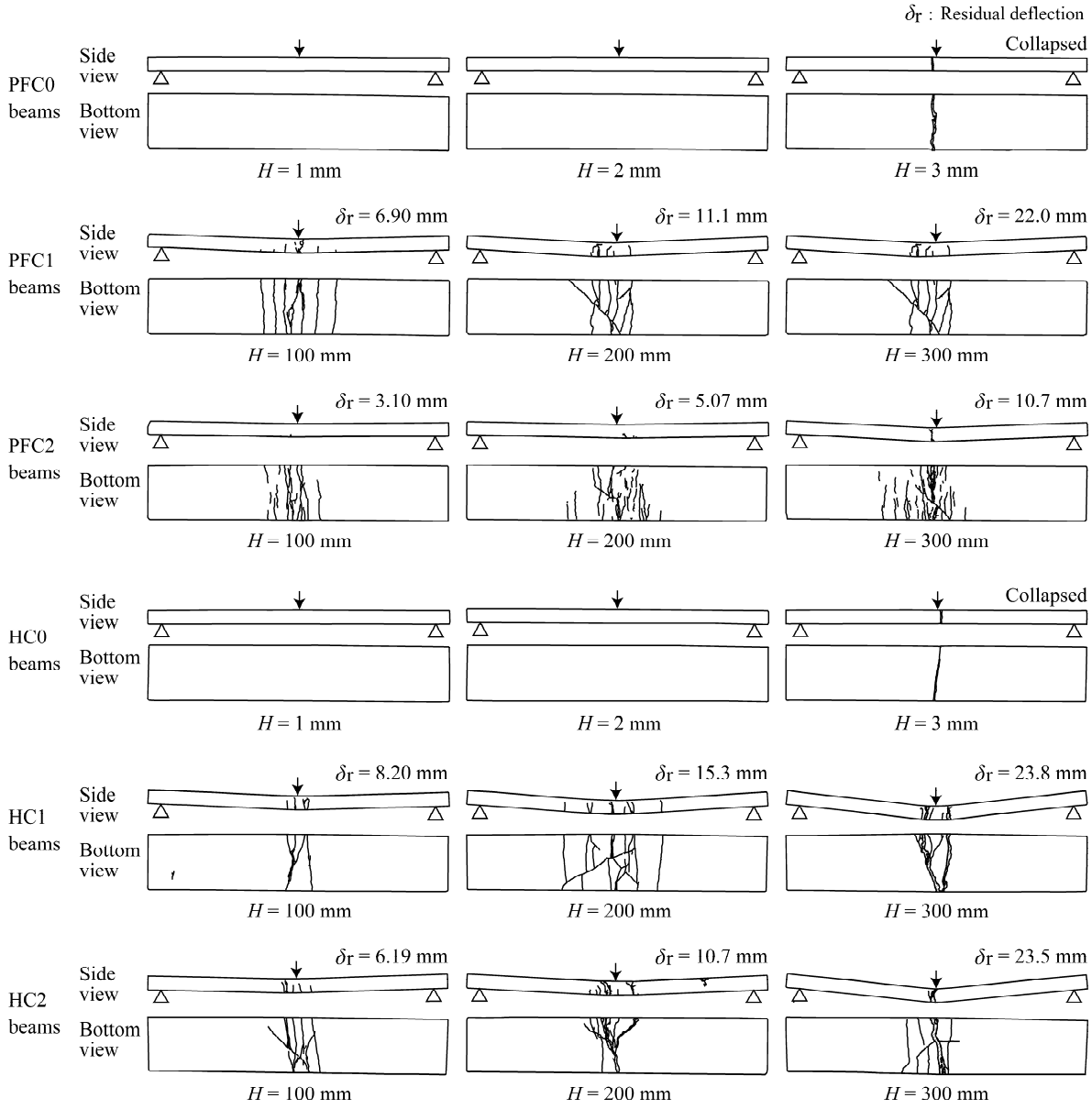

Fig. 10 Crack distribution after completion of experiment.

that the crack dispersion effect by the mixture of fibers is more efficiently exhibited and the residual deflection is smaller than that in the other beams. As the bending cracks near the loading point reach the upper edge of the beam, it is considered that tensile stress acts on the entire cross section of the beam at the maximum response. Therefore, it is considered that the tensile properties after cracking are much more important than the compressive strength for the high impact resistance of the fiber-reinforced PFC beam. Thus, the bonding resistance between PFC and steel fibers is also expected to contribute greatly to the improvement of tensile toughness performance.

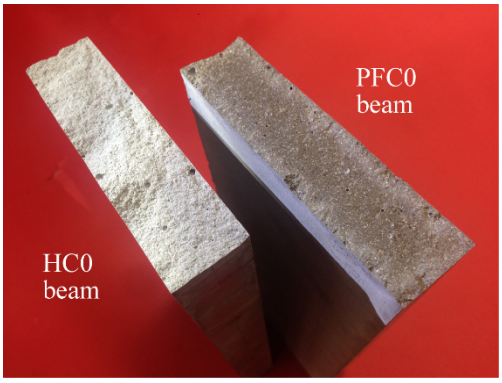

Fig. 11 Crack surface of PFC/HC0 beams.

4.3 Crack progression

Figure 13 shows the progress of cracking of the fiber-reinforced PFC/HC beam at H = 300 mm. Here, it is shown at intervals of 5 ms from the elapsed time t = 5 ms after the weight collision to t = 25 ms, which indicates the maximum deflection and it can be seen that the

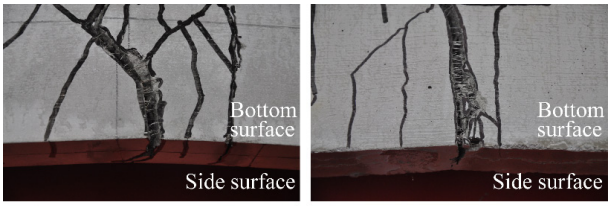

(a) HC1-H300 (b) HC2-H300

Fig. 12 Crack opening condition on bottom surface of HC1/2-H300.

(a) PFC1-H300 (b) PFC2-H300 (c) HC1-H300 (d) HC2-H300

Fig. 13 Progression of cracking.

loading point deflection and the width of the bending cracks increase with the passage of time. In addition, one or two bending cracks are generated near the loading point, and progress from the lower surface of the beam toward the upper surface. Subsequently, those cracks almost reach the upper surface at t = 10 ms. After t = 20 ms, it can be seen that small pieces and particles are falling from the widely opened cracks. In the case of PFC2-H300, it is clear that the deformation amount and crack width are smaller than those of the other specimens. Because PFC2-H300 has the largest static bending strength, it is seen that the tendency of the impact-resistant performance corresponds to that of the static load-carrying capacity. In HC1-H300, two cracks near the loading point may be due to the influence of the weight diameter.

Figure 14 shows the transition of the relative distance of the target marker (hereinafter, relative distance) found in the high-speed camera image of **Fig. 13** as a time-history waveform. The relative distance was evaluated by determining the distance between the loading point and the target markers on the left and right sides by image analysis. The relative distance of the target marker was evaluated as an index of the width of the bending crack, since the cracks are wide open in all the specimens. From the figure, it is seen that the relative distance after weight collision increases and it remains after reaching the maximum response. These waveform characteristics roughly correspond to the loading point deflection waveform shown in **Fig. 9**. The bending crack of PFC2-H300 is the smallest, and its maximum value is about 1 mm. According to Yanagida *et al.* (2016), in the tensile softening curve of PFC with a steel fiber content of 2 vol.% [see **Fig. 3(c)**], the crack mouth opening width capable of holding a constant tensile stress after cracking is less than about 1 mm. It can be expected that, after the impact-loading test, PFC2-H300 retains almost the same bending capacity as that immediately after cracking.

4.4 Loading point deflection and relative distance

Figure 15 shows the maximum and residual deflections, and the maximum and residual relative distances at each drop height H. The relative distance was evaluated by adding the values on the left and right sides of the loading point. From these figures, it is understood that the deflection and relative distance tend to increase as the drop height increases for all specimens. In addition, PFC1 and HC1/2 beams tend to increase in deflection and relative distance at H = 300 mm. On the other hand, in the case of the PFC2 beam, this tendency is not no-

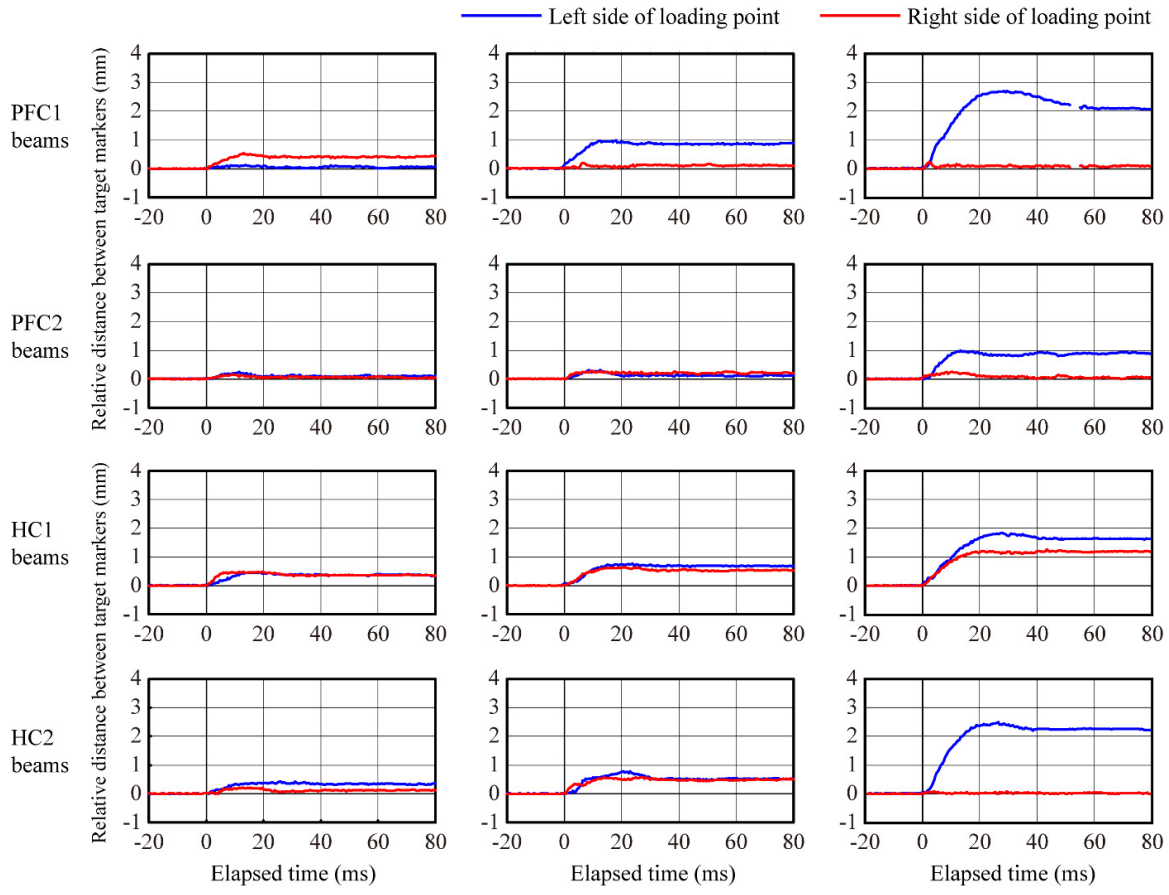

(a) H = 100 mm (b) H = 200 mm (c) H = 300 mm

Fig. 14 Time-history waveform of relative distance of target marker.

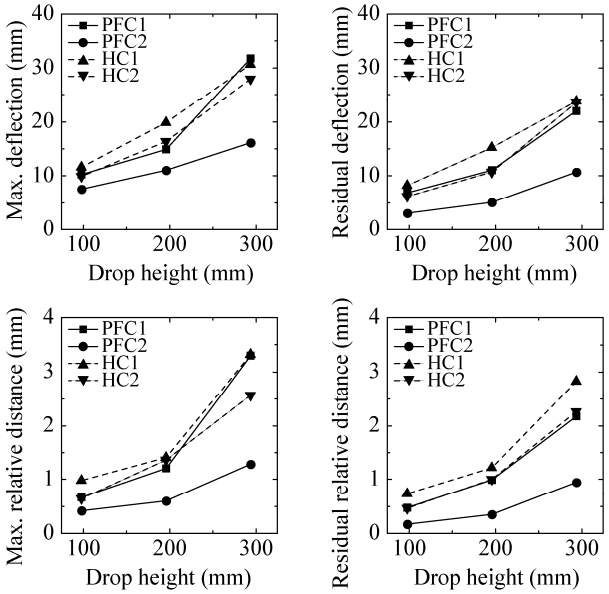

Fig. 15 Relationship between response value and drop height.

ticeable. This means that the PFC1 and HC1/2 beams were angularly broken around the loading point, but the PFC2 beam was slightly deformed. This means that the cracks of the PFC2 beam were dispersed and the beam did not collapse, as shown in the crack diagram (**Fig. 10**) and the progress of the cracking (**Fig. 13**).

Thus, in this experiment, it was found that the static bending strength and impact resistance performance were dramatically improved by mixing 2 vol.% of steel fiber into the PFC.

5. Conclusions

The authors investigated the impact resistance behavior of steel-fiber-reinforced PFC through falling-weight impact tests conducted on PFC formed into a beam shape. The results obtained from this study are summarized below.

(1) In the case of the static loading test, the load-carrying capacity and crack dispersion effect of the fiber-reinforced PFC beam were found to be higher than those of the HC beam even under large deflections. This means that the fine microstructure of the matrix of PFC can improve the bonding resistance of the steel fiber.
(2) The flexural rigidity of the beams under impact loading can be improved by increasing the steel-fiber content, irrespective of the type of concrete.
(3) The impact-resistant performance of the PFC beam as well as its static load-carrying capacity are significantly improved by mixing 2 vol.% of steel fibers.
(4) The crack opening width of the concrete beam under impact loading is smallest when 2 vol.% of steel fiber is mixed in PFC. In addition, the cracking dispersion effect is also high. This means that the bonding resistance between PFC and steel fibers contributes substantially to the improvement of tensile toughness performance.
(5) When the crack opening width of the concrete beam under impact loading was about 1 mm or less, the beam did not experience significant angular breakage. This result is related to the characteristics of the tensile softening curve of PFC.

Furthermore, in this research, all test specimens were broken by tensile stress acting on the entire cross section. As a result, the ultra-high strength properties of PFC were not definitively exhibited. Therefore, we believe that it would be necessary to study members combining tensile reinforcement, such as rebar, prestressed-concrete steel, and fiber-reinforced polymer. In the future, PFC could be used as an effective strengthening material for impact-resistant structures.

Acknowledgment

In conducting this research, the Civil Engineering Research Institute of the Cold Region provided support by lending high-speed cameras and providing invaluable advice on usage. In addition, we are grateful to the graduate students and undergraduates in the Structural Mechanics Laboratory at Muroran Institute of Technology, who provided support at all stages, from experiment setup to data arrangement. This work was supported by JSPS KAKENHI Grant Number 19H02394. We would like to thank Editage, Cactus Communications Ltd., Tokyo for English language editing.

References

Beppu, M., Ogawa, A. and Takahashi. J., (2016). "Impact resistant performance of fiber reinforced cementitious composite plates subjected to high velocity impact by a rigid projectile." *Journal of Japan Society of Civil Engineers, Ser. E2 (Materials and Concrete Structures)*, 70(2), 180-193. (in Japanese)

Beppu, M., Mutou, S. and Takahashi, J., (2013). "A fundamental study on evaluation methods on the local damage of ultra high strength or reinforced concrete plates subjected to high velocity impact." *Journal of Structural Engineering*, 59A, 1037-1047. (in Japanese)

Fujikake, K., Senga, T., Ueda, N., Ohno, T. and Katagiri, M., (2006a). "Effects of strain rate on tensile behavior of reactive powder concrete." *Journal of Advanced Concrete Technology*, 4(1), 79-84.

Fujikake, K., Senga, T., Ueda, N., Ohno, T. and Katagiri, M., (2006b). "Nonlinear analysis for reactive powder concrete beams under rapid flexural loadings." *Journal of Advanced Concrete Technology*, 4(1), 85-97.

Fujikake, K., Senga, T., Ueda, N., Ohno, T. and Katagiri, M., (2006c). "Study on impact response of reactive powder concrete beam and its analytical model." *Journal of Advanced Concrete Technology*, 4(1), 99-108.

JCI, (2012). "*JCI-C82: Proceedings of innovative application of fiber reinforced cementitious composites*."

Tokyo: Japan Concrete Institute. (in Japanese)

JSCE, (2015). "*Report of research subcommittee for structural use of fiber reinforced concrete (Concrete technology series 106)*." Tokyo: Japan Society of Civil Engineers. (In Japanese)

JSCE, (2004). "*Design and construction guidelines for ultra-high strength fiber reinforced concrete (Concrete library 113, draft)*." Japan Society of Civil Engineers. (In Japanese)

JSDFE, (2018). "*Assessment guideline for the local failure of structures subjected to impact actions*." Tokyo: Japan Society of the Defense Facility Engineers. (in Japanese)

JIS, (2018). "*JIS A 1108 2018 Method of test for compressive strength of concrete*." Tokyo: Japanese Standards Association.

Kabele, P., Sajdlová, T., Rydval, M. and Kolísko, J., (2015). "Modeling of high-strength FRC structural elements with spatially non-uniform fiber volume fraction." *Journal of Advanced Concrete Technology*, 13(6), 311-324.

Kono, K., Nakayama, R. and Tada, K., (2015). "A new cement-hardened material that exhibits a compressive strength of 460 N/mm^2 in conventional pour molding." In: *Proceedings of the 24th Symposium on Developments in Prestressed Concrete*, Toyama, Japan 22-23 October 2015. Tokyo: Japan Prestressed Concrete Institute, 24, 545-550. (in Japanese)

Kono, K., Mori. K., Tada, K. and Tanaka. T., (2016a). "Development of the world's highest strength concrete and possibility of further performance improvement." *Concrete Journal*, 54(7), 702-709. (in Japanese)

Kono, K., Nakayama, R., Tada, K. and Tanaka, T., (2016b). "Manufacturing method of cement-based material which shows compressive strength of 450 N/mm^2 or more and change of hardened structure." *Proceedings of the Japan Concrete Institute*, 38(1), pp. 1443-1448 (in Japanese)

Limpaninlachat, P., Nakamura, T., Kono, K. and Niwa, J., (2017). "Shear strengthening performance of post-tensioned UFC panel on reinforced concrete beams." *Journal of Advanced Concrete Technology*, 15(9), 558-573.

Ma, Z., Zhao, T. and Yao, X., (2016). "Influence of applied loads on the permeability behavior of ultra high performance concrete with steel fibers." *Journal of Advanced Concrete Technology*, 14(12), 770-781.

Sugano, S., Kimura, H. and Shirai, K., (2007). "Study of new RC structures using ultra-high-strength fiber-reinforced concrete (UFC) - the challenge of applying 200 MPa UFC to earthquake resistant building structures." *Journal of Advanced Concrete Technology*, 5(2), 133-147.

Takahashi, J. and Beppu, M., (2013). "Experimental study on reinforcing effects by UFC panel under high velocity impact loading." *Proceedings of the Concrete Structure Scenarios*, 13, 405-412. (in Japanese)

Takemoto, S., Konno, H., Mikami, H. and Matsuoka, K., (2000). "Prototype impact test on impact resistant upgrading effects of AFRP sheet jacketing method for PC snow-sheds." *Proceedings of the Japan Concrete Institute*, 22(1), 505-510. (in Japanese)

Ueno, H., Beppu, M. and Ogawa, A., (2015). "Effects of mixing ratio of short fibers in PVA fiber reinforced cementitious composite plates on their impact resistant performance subjected to high velocity impact." *Journal of Structural Engineering*, 61A, 899-911. (in Japanese)

Ueno, H., Beppu, M., Ichino, H., Musha, H. and Okamoto, S., (2017). "An experimental study on the local failure of ultra high strength fiber reinforced concrete panels subjected to high velocity impact of deformable projectiles." *Journal of Structural Engineering*, 63A, 1149-1162. (in Japanese)

Walraven, J., (2009). "High performance concrete: a material with a large potential." *Journal of Advanced Concrete Technology*, 7(2), 145-156.

Yanagida, K., Nakamura, T., Kono, K. and Niwa, J., (2016). "Mechanical properties of fiber reinforced concrete using closest packed matrix with compressive strength of 400 N/mm^2." *Proceedings of the Japan Concrete Institute*, 38(1), 279-284. (in Japanese)